Progress In Electromagnetics Research, PIER 78, 285–300, 2008

RADIATION FROM OPEN-ENDED CIRCULAR WAVEGUIDES: A FORMULATION BASED ON THE INCOMPLETE HANKEL FUNCTIONS

R. Cicchetti

Department of Electronic Engineering
University of Rome "La Sapienza"
Via Eudossiana, Rome 18-00184, Italy

A. Faraone

Motorola, Inc.
Corporate EME Research Laboratory
8000 West Sunrise Blvd., Fort Lauderdale, FL 33322, USA

Abstract—An analytical formulation based on physical optics is employed to determine the field and the radiated power distribution by open-ended circular waveguides. Using the incomplete Hankel functions, the line integrals yielding the electromagnetic field are evaluated in closed analytical form along the waveguide axis. It is shown that cylindrical waves are generated by the surface currents flowing on the waveguide walls, while spherical waves are produced by the currents and charges excited at the waveguide truncation. Cylindrical and spherical waves are shown to be responsible for the field synthesis in terms of waveguide modes and scattered fields at the waveguide mouth. Numerical results concerning the spatial distribution of the electromagnetic field and associated power density are compared with previously published results, showing the advantage of the incomplete Hankel functions formulation. Finally, the uniform asymptotic representation of the incomplete Hankel function is shown to be suitable to compute the field distribution on the waveguide axis except for the TE_{11} and TM_{01} modes.

1. INTRODUCTION

The electromagnetic analysis of semi-infinite open-ended waveguides, is a relevant canonical problem in applied electromagnetics since they can represent waveguide antennas [1, 2], reflector antenna feeders [3–6], and scatterers in radar cross section analysis [7–11]. The exact solution of the electromagnetic field excited in open-ended circular waveguides can be derived using the *Wiener-Hopf* technique. This technique, that is only applicable to circular waveguides [12], allows expressing the field quantities in terms of spectral Fourier integrals. Consequently, to obtain the corresponding expressions in the coordinate domain, the evaluation of slowly converging numerical integrations is required. On the other hand, asymptotic techniques fail to describe the field along or near the waveguide axis [6]. Physical optics (PO) may indeed allow computing the field with sufficient numerical accuracy [7, 8], therefore, in this paper, the explicit expressions of the PO electromagnetic field components excited along the axis of circular waveguides are derived in closed form. The field is expressed in terms of incomplete Hankel functions ($IHFs$), recently introduced in literature [13–15], which provide physical insight into the wave propagation and radiation mechanisms. This representation further allows establishing the spatial regions where asymptotic techniques fail.

The paper, which completes and extends the results presented in [15], consists of five sections. In Section 2, the procedure adopted to evaluate the PO field quantities is summarized, while in Section 3 the electromagnetic field components are derived, in closed analytical form, along the waveguide axis. The resulting expressions, which comprise radiative, inductive and electrostatic terms, are then related with the Brillouin's angles. The latter are linked with the Keller's cone associated with the scattered field phenomenon. Numerical results concerning the spatial behavior of fields and power density in truncated circular waveguides excited by TE and TM traveling wave modes are presented in Section 4, while a concluding discussion is outlined in Section 5.

2. METHODOLOGY

A cylindrical reference frame (ρ, ϕ, z), with unit vectors $\hat{\boldsymbol{\rho}}$, $\hat{\boldsymbol{\phi}}$, and $\hat{\boldsymbol{z}}$, is adopted to express the field quantities, while a time dependence $e^{j\,\omega\,t}$, with ω being the angular frequency, is assumed and suppressed.

An open-ended circular waveguide having radius a, truncated at z_0, is shown in Fig. 1. As discussed in [15], the electromagnetic field distribution excited in the structure can be evaluated by means

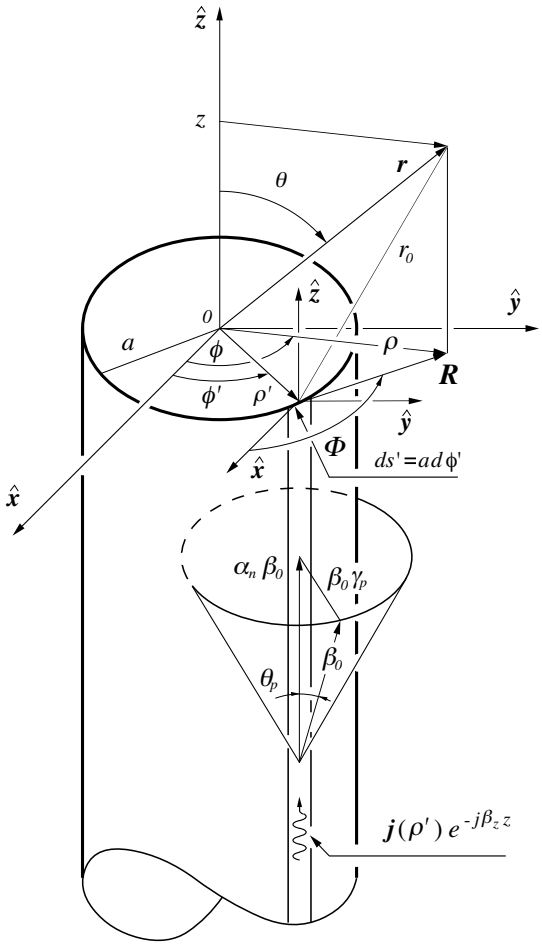

Figure 1. A truncated circular waveguide excited by a guided-wave mode. The reference system adopted to define the field quantities is established.

of the surface currents excited on the metal surface using the *PO* approximation. Doing so, and adopting the procedure presented in [15], it is possible to reduce the *PO* surface integrals in simple line integrals along the waveguide contour as follows

$$\boldsymbol{E}(\boldsymbol{\rho}, z, z_0) = \int_0^{2\pi} \underline{\boldsymbol{T}}(\phi') \cdot \underline{\boldsymbol{G}}_E(\boldsymbol{\rho}, z, z_0, \phi') \cdot \boldsymbol{j}(\phi') a d\phi', \qquad (1)$$

$$\boldsymbol{H}(\boldsymbol{\rho}, z, z_0) = \int_0^{2\pi} \underline{\boldsymbol{T}}(\phi') \cdot \underline{\boldsymbol{G}}_H(\boldsymbol{\rho}, z, z_0, \phi') \cdot \boldsymbol{j}(\phi') a d\phi', \tag{2}$$

where $\boldsymbol{j}(\phi)$ is the PO surface current, while $\underline{\boldsymbol{G}}_E(\cdot)$, $\underline{\boldsymbol{G}}_H(\cdot)$, and $\underline{\boldsymbol{T}}(\cdot)$ are the tensors defined in [15].

The integrals (1)–(2), which include the PO edge currents that take into account the near-field effects, express the field synthesis in terms of waveguide modes and scattered fields at the waveguide mouth, anywhere inside and outside the waveguide. Waveguide modes are synthesized by means of a superposition of cylindrical waves expressed through the Hankel functions embedded in the $IHFs$ [13, Eq. (37)], while the scattered field is synthesized by the current and charge excited at the waveguide truncation as well as by the $IHFs$ end-point contribution modeling the transition of said cylindrical waves into spherical ones.

2.1. The Field and the Power Density along the Waveguide Axis

As observed in [15], along the waveguide axis the tensors components reported in (1)–(2) become independent of the source angle, while those of the transformation matrix $\underline{\boldsymbol{T}}$ [15, Eq. (10)] become proportional to trigonometric functions of the difference between the source and observation angles [15, Eqs. (17)–(18)]. Using the results reported in [15] it is possible to express the propagating modes with non vanishing transverse field components along the waveguide axis. These modes, having $m = 1$ can be expressed as follows

$$E_\rho(\rho, \phi, z; z_0)|_{\rho=0} = \pi a \left[g^E_{Rz}(a, z; z_0)\, h_{\phi\,\max} - g^E_{\Phi\Phi}(a, z; z_0)\, h_{z\,\max} \right] \sin(\phi + \phi_0), \tag{3}$$

$$E_\phi(\rho, \phi, z; z_0)|_{\rho=0} = \pi a \left[g^E_{Rz}(a, z; z_0)\, h_{\phi\,\max} - g^E_{\Phi\Phi}(a, z; z_0)\, h_{z\,\max} \right] \cos(\phi + \phi_0), \tag{4}$$

$$E_z(\rho, \phi, z; z_0)|_{\rho=0} = 0, \tag{5}$$

and

$$H_\rho(\rho, \phi, z; z_0)|_{\rho=0} = -\pi a \left[g^H_{\Phi z}(a, z; z_0)\, h_{\phi\,\max} + g^H_{R\Phi}(a, z; z_0)\, h_{z\,\max} \right] \cos(\phi + \phi_0), \tag{6}$$

$$H_\phi(\rho, \phi, z; z_0)|_{\rho=0} = \pi a \left[g^H_{\Phi z}(a, z; z_0)\, h_{\phi\,\max} + g^H_{R\Phi}(a, z; z_0)\, h_{z\,\max} \right] \sin(\phi + \phi_0), \tag{7}$$

$$H_z(\rho, \phi, z; z_0)|_{\rho=0} = 0 \tag{8}$$

where the functions $g^E_{Rz}(\cdot)$, $g^E_{\Phi\Phi}(\cdot)$, $g^H_{\Phi z}(\cdot)$, and $g^H_{R\Phi}(\cdot)$ are defined through the following relationships

$$g^E_{Rz}(R,z;z_0) = \frac{1}{j\omega\varepsilon_0}\frac{\partial^2}{\partial R\partial z}A_0^{\pm}(R,z,z_0) \tag{9}$$

$$g^E_{\Phi\Phi}(R,z;z_0) = j\omega\mu_0\left[1+\frac{1}{\beta_0^2}\frac{1}{R}\frac{\partial}{\partial R}\right]A_0^{\pm}(R,z,z_0) \tag{10}$$

and

$$g^H_{\Phi z}(R,z;z_0) = -\frac{\partial}{\partial R}A_0^{\pm}(R,z,z_0), \tag{11}$$

$$g^H_{R\Phi}(R,z;z_0) = \frac{\partial}{\partial z}A_0^{\pm}(R,z,z_0), \tag{12}$$

with

$$A_0^{\pm}(R,z,z_0) = -j\frac{1}{4}H_0^{(2)}\left[\beta_0\gamma_p R, \sinh^{-1}\left(\frac{\Delta z \mp \alpha_n r_0}{\gamma_p R}\right)\right]e^{\mp j\beta_z z}, \tag{13}$$

where β_0 and β_z are the free-space and the guided wave wavenumbers, respectively. The function $H_0^{(2)}[\cdot]$ in (13) is the *incomplete* Hankel function of second kind and order zero [13], whose arguments are: $\alpha_n = \frac{\beta_z}{\beta_0}$, $\gamma_p = \sqrt{1-\alpha_n^2}$, $\Delta z = z - z_0$, and $r_0 = \sqrt{R^2+(\Delta z)^2}$. The partial derivative appearing in (9)–(13) are reported in Appendix A. The magnetic field components in (3)–(8) are those describing the surface current in the corresponding unlimited waveguide (*PO* approximation). For TE-modes they are

$$h^{TE}_{\phi\,\max} = \pm j\alpha_n\frac{\beta_0 a}{(\xi'_{1n})^2}C_0 J_1(\xi'_{1n}), \tag{14}$$

$$h^{TE}_{z\,\max} = C_0 J_1(\xi'_{1n}), \tag{15}$$

where $J_1(\cdot)$ is the Bessel function of the first kind of order $m=1$, and ξ'_{1n} is the n-th zero of its first derivative, while for TM-modes we have

$$h^{TM}_{\phi\,\max} = -j\frac{\omega\varepsilon_0}{\zeta_{1n}}aC_0 J'_1(\zeta_{1n}) \tag{16}$$

ζ_{1n} being the n-th zero of the function $J_1(\cdot)$. Finally, C_0 is a constant which depends on the impinging field amplitude.

Using (3)–(8), the expressions for the fields associated to the

progressive waveguide modes are finally derived

$$
\begin{aligned}
&E_\rho\left(\rho,\phi,z;z_0\right)\big|_{\rho=0} = \\
&\pi a\left\{\frac{1}{4}\left[\omega\mu_0 H_0^{(2)}\left[\beta_0\gamma_p a, sinh^{-1}\left(\frac{\Delta z-\alpha_n r_0}{\gamma_p a}\right)\right]h_{z\max}\right.\right. \\
&-\gamma_p\frac{\eta_0}{a}H_1^{(2)}\left[\beta_0\gamma_p a, sinh^{-1}\left(\frac{\Delta z-\alpha_n r_0}{\gamma_p a}\right)\right]h_{z\max} \\
&\quad\left.-j\omega\mu_0\alpha_n\gamma_p H_1^{(2)}\left[\beta_0\gamma_p a, sinh^{-1}\left(\frac{\Delta z-\alpha_n r_0}{\gamma_p a}\right)\right]h_{\phi\max}\right]e^{-j\beta_z z} \\
&+\left[-\eta_0\alpha_n\frac{\Delta z}{a}\frac{e^{-j\beta_0 r_0}}{4\pi r_0}+\frac{a}{j\omega\varepsilon_0}\left(j\beta_0+\frac{1}{r_0}\right)\frac{e^{-j\beta_0 r_0}}{4\pi r_0^2}\right]h_{\phi\max}e^{-j\beta_z z_0} \\
&\left.-\frac{1}{j\omega\varepsilon_0}\frac{\Delta z}{a^2}\frac{e^{-j\beta_0 r_0}}{4\pi r_0}e^{-j\beta_z z_0}h_{z\max}\right\}\sin(\phi+\phi_0)
\end{aligned}
\tag{17}
$$

$$
\begin{aligned}
&E_\phi\left(\rho,\phi,z;z_0\right)\big|_{\rho=0} = \\
&\pi a\left\{\frac{1}{4}\left[\omega\mu_0 H_0^{(2)}\left[\beta_0\gamma_p a, sinh^{-1}\left(\frac{\Delta z-\alpha_n r_0}{\gamma_p a}\right)\right]h_{z\max}\right.\right. \\
&-\gamma_p\frac{\eta_0}{a}H_1^{(2)}\left[\beta_0\gamma_p a, sinh^{-1}\left(\frac{\Delta z-\alpha_n r_0}{\gamma_p a}\right)\right]h_{z\max} \\
&\quad\left.-j\omega\mu_0\alpha_n\gamma_p H_1^{(2)}\left[\beta_0\gamma_p a, sinh^{-1}\left(\frac{\Delta z-\alpha_n r_0}{\gamma_p a}\right)\right]h_{\phi\max}\right]e^{-j\beta_z z} \\
&+\left[-\eta_0\alpha_n\frac{\Delta z}{a}\frac{e^{-j\beta_0 r_0}}{4\pi r_0}+\frac{a}{j\omega\varepsilon_0}\left(j\beta_0+\frac{1}{r_0}\right)\frac{e^{-j\beta_0 r_0}}{4\pi r_0^2}\right]h_{\phi\max}e^{-j\beta_z z_0} \\
&\left.-\frac{1}{j\omega\varepsilon_0}\frac{\Delta z}{a^2}\frac{e^{-j\beta_0 r_0}}{4\pi r_0}e^{-j\beta_z z_0}h_{z\max}\right\}\cos(\phi+\phi_0)
\end{aligned}
\tag{18}
$$

and

$$
\begin{aligned}
&H_\rho\left(\rho,\phi,z;z_0\right)\big|_{\rho=0} = \\
&\pi a\left\{\frac{1}{4}\left[j\beta_0\gamma_p H_1^{(2)}\left[\beta_0\gamma_p a, sinh^{-1}\left(\frac{\Delta z-\alpha_n r_0}{\gamma_p a}\right)\right]h_{\phi\max}\right.\right. \\
&+\beta_0\alpha_n H_0^{(2)}\left[\beta_0\gamma_p a, sinh^{-1}\left(\frac{\Delta z-\alpha_n r_0}{\gamma_p a}\right)\right]h_{z\max}\left.\right]e^{-j\beta_z z} \\
&\left.+\left[\frac{\Delta z}{a}h_{\phi\max}+h_{z\max}\right]\frac{e^{-j\beta_0 r_0}}{4\pi r_0}e^{-j\beta_z z_0}\right\}\cos(\phi+\phi_0)
\end{aligned}
\tag{19}
$$

$$
\begin{aligned}
&H_\phi(\rho,\phi,z;z_0)|_{\rho=0} = \\
&-\pi a\left\{\frac{1}{4}\left[j\beta_0\gamma_p H_1^{(2)}\left[\beta_0\gamma_p a, sinh^{-1}\left(\frac{\Delta z-\alpha_n r_0}{\gamma_p a}\right)\right]h_{\phi\max}\right.\right. \\
&+\beta_0\alpha_n H_0^{(2)}\left[\beta_0\gamma_p a, sinh^{-1}\left(\frac{\Delta z-\alpha_n r_0}{\gamma_p a}\right)\right]h_{z\max}\Bigg]e^{-j\beta_z z} \\
&\left.+\left[\frac{\Delta z}{a}h_{\phi\max}+h_{z\max}\right]\frac{e^{-j\beta_0 r_0}}{4\pi r_0}e^{-j\beta_z z_0}\right\}\sin(\phi+\phi_0) \qquad (20)
\end{aligned}
$$

showing that the electromagnetic field is described by means of incomplete Hankel functions of order zero and one that model the transition from the guided toward the spherical wave propagation regime, as well as additional spherical wave contributions arising from the waveguide truncation. Moreover, they explicitly show the dependence from the parameters α_n and γ_p. These parameters, whose expressions in terms of the zeroes ζ_{1n} of $J_1(\cdot)$ or those of $J_1'(\cdot)$ (ξ_{1n}') are

$$\alpha_n = \sqrt{1-\left(\frac{p_{1n}}{\beta_0 a}\right)^2} \qquad (21)$$

$$\gamma_n = \frac{p_{1n}}{\beta_0 a} \qquad (22)$$

where

$$p_{1n} = \begin{cases} \xi_{1n}' & \text{for } TE \text{ modes} \\ \zeta_{1n} & \text{for } TM \text{ modes} \end{cases}, \qquad (23)$$

are related with the Brillouin's angles (see Tabs. 1 and 2), which coincides with the semi-aperture angle of the Keller's cone (see Fig. 1). The field expressions (17)–(20) can also be employed to compute the z-component of the Poynting vector (P_z) excited along the waveguide axis. For the TE_{0n} and TM_{0n} modes the z-component of the Poynting vector vanishes since they present only the longitudinal components different from zero along the z-axis. Indeed, for the sake of completeness, the analytical expressions of these modes are reported in Appendix B. These expressions have the same analytical structures as Eqs. (17)–(20).

It is worth reminding that the $IHFs$ appearing in (17)–(20) possess the asymptotic representation introduced in [13]. This representation is numerically very accurate when the $IHFs$ parameter $\Omega > 3$ [13, Eq. (48)], where $\Omega = \beta_0\gamma_p a = p_{1n}$ (see Eq. (22)). It is easily verified that this condition is met for all the waveguide modes,

Table 1.

Characteristic parameters dependence on the guide radius for TE_{11} mode				
Guide radii	α_n	γ_p	*Brillouin angle*	*Half amplitude field point* z_{half}/λ_0
$0.5\lambda_0$	0.810263	0.586066	35.8784°	0.691272
λ_0	0.956102	0.293034	17.0397°	3.26277
$2\lambda_0$	0.989208	0.146518	8.42512°	13.5029
$4\lambda_0$	0.997313	0.0732583	4.20116°	54.4546
$10\lambda_0$	0.999571	0.0293033	1.6792°	341.111

Table 2.

Characteristic parameters dependence on the guide radius for TM_{11} mode				
Guide radii	α_n	γ_p	*Brillouin angle*	*Half amplitude field point* z_{half}/λ_0
λ_0	0.792528	0.609836	37.5776°	1.29958
$2\lambda_0$	0.952379	0.304917	17.7532°	6.24681
$4\lambda_0$	0.988310	0.152458	8.76944°	25.9301
$10\lambda_0$	0.998139	0.0609835	3.49605°	163.674

except for the TE_{11} and TM_{01}, for which $\Omega = \xi'_{11} = 1.8412$ and $\Omega = \zeta_{01} = 2.4049$, respectively. This will be clearly shown by the numerical results reported in the next section.

3. NUMERICAL RESULTS

In this section, numerical results concerning the field and power distributions excited in open-ended circular waveguides are presented. The validation of the numerical procedure adopted herein for the evaluation of the field quantities has been performed in [15]. So, in this section we report comparisons with previously published results and characterize the field and the power density distribution excited along the axis of circular waveguides. We will consider the excitation of the progressive guided wave only, and the waveguide truncation will be assumed at $z_0 = 0$. Neglecting the reflected wave introduces a small error since the modal reflection coefficients for these truncated waveguide structures are typically small [5]. A full-wave analysis would entail a laborious MoM approach encompassing modal basis function, or a hybrid PO/MoM formulation with suitable basis functions located

near the waveguide truncation.

In order to compare our formulation with others in literature, we analyzed the field pattern of the open-ended circular waveguide analyzed in [6], having radius $a = 0.5\lambda_0$, and excited by the fundamental TE_{11}-mode. The angular behavior of the ϕ-component of the electric field, computed in the E-plane at $r = 0.7\lambda_0$ and $r = 1.5\lambda_0$, is shown in Fig. 2 where it is compared against analogous results obtained by means of the asymptotic solution proposed in [6]. An excellent agreement between the two normalized patterns is observed. It should be remarked that we extended the angular range to about 180°, thus penetrating the waveguide wall and reaching the waveguide axis. As discussed in [14, 15] asymptotic techniques can fail to represent the field excited inside the waveguide or in its proximity. The formulation based on the $IHFs$, instead, allows overcoming such a limitation. Moreover, the numerical accuracy of the asymptotic technique tends to decrease for waveguides having electrically large cross-sections.

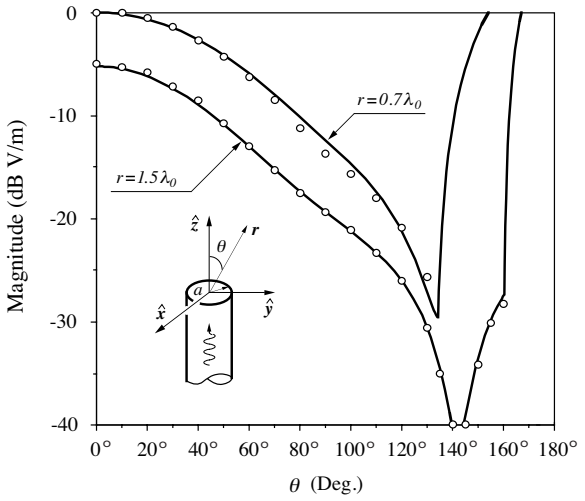

Figure 2. Magnitude of the ϕ-component of the electric field (H-plane) radiated by a truncated circular waveguide versus elevation angle θ. Guide characteristics: $a = 0.5\lambda_0$, exciting mode: TE_{11}. The empty circles trace the asymptotic solution presented in [6]. Curves normalized with respect to the maximum value at broadside for $r = 0.7\lambda_0$. The cuspid in both curves is where the field point crosses the waveguide wall.

In Figs. 3(a)–3(b), the spatial behavior along the waveguide axis of the radial component of the electric field in the E-plane, and that of the radial component of the magnetic field in the H-plane, are reported for the case of a circular waveguide having radius $a = 2\lambda_0$ excited with the TE_{11}-mode. The field amplitudes have been computed starting from the internal waveguide region up to the far-field region and normalized so that the peak level of the $\rho-$component of the exciting TE_{11}-mode

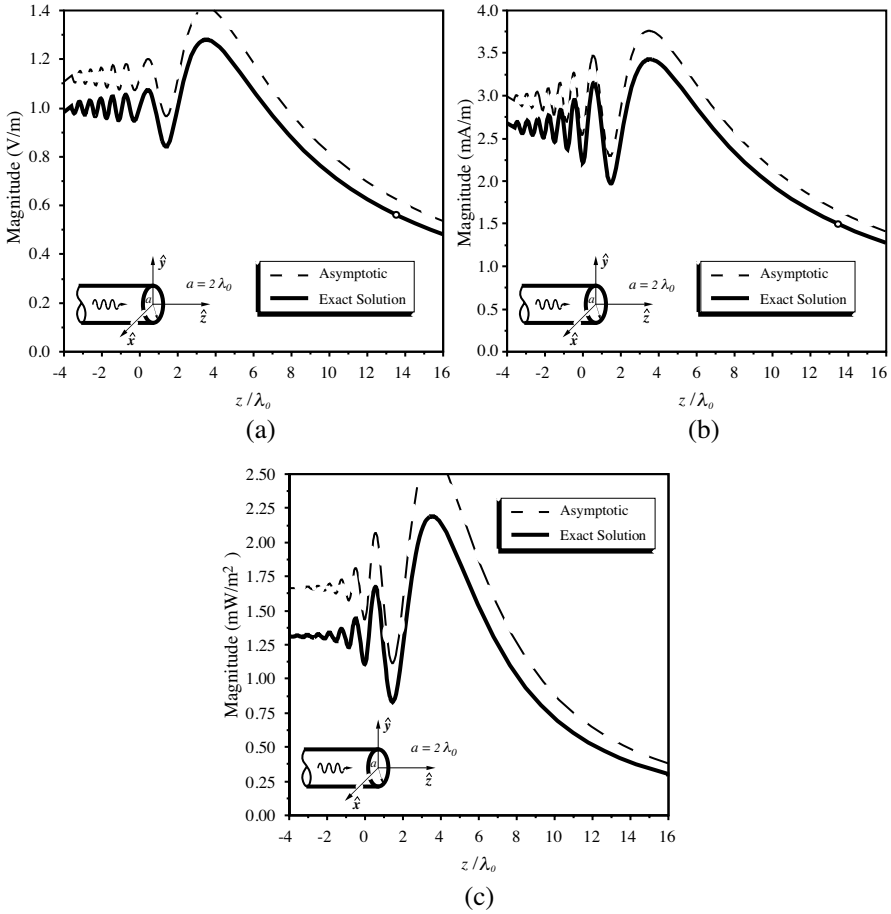

Figure 3. Field quantities of the TE_{11} mode along the z-axis of a truncated circular waveguide ($a = 2\lambda_0$, $z_0 = 0$). (a) $|E_\rho|$ in the E-plane, (b) $|H_\rho|$ in the H-plane, and (c) $|P_z|$. The accuracy of the asymptotic solution is marginal as expected based on the theory. The circle indicates the point z_{half}.

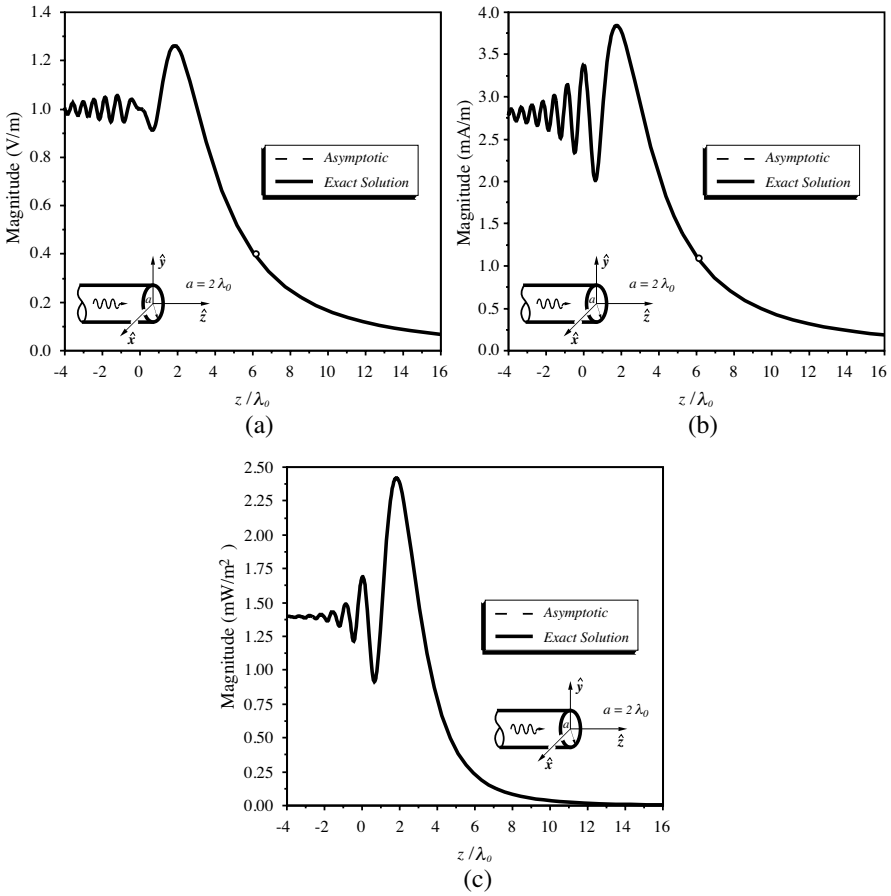

Figure 4. Field quantities of the TM_{11} mode along the z-axis of a truncated circular waveguide ($a = 2\lambda_0$, $z_0 = 0$). (a) $|E_\rho|$ in the E-plane, (b) $|H_\rho|$ in the H-plane, and (c) $|P_z|$. The accuracy of the asymptotic solution is excellent since the dotted and solid lines coincide. The circle indicates the point z_{half}.

electric field is 1 V/m. Finally, in Fig. 3(c) the z-component of the Poynting vector is reported for completeness. These figures show the interaction of the guided wave with the field scattered at the open-end discontinuity, producing the undulations that are observed near the waveguide truncation. The distance where the field amplitude overshoot is observed, corresponding to the field character transition toward the spherical wave propagation regime [14], moves away from

the waveguide aperture as its electrical cross-section increases, and so does the parameter z_{half} (see Tabs. 1 and 2), i.e., the point where the electromagnetic field amplitude on the waveguide axis decays to one half [15]. The same point identifies the maximum extension of the geometrical optics field along the z-axis. From Eqs. (17)–(20) it is evident that the field focusing (overshoot) phenomenon is caused by the field scattered at the waveguide truncation. A similar behavior is observable when the considered guides are excited by means of a TM_{11}-mode. The corresponding case for $a = 2\lambda_0$ is reported in Fig. 4. Finally, it should be observed that the field quantities computed using the asymptotic representation of the $IHFs$ show the inadequacy in producing accurate results along the waveguide axis only for the TE_{11}-mode (see Figs. 3–4). In any case, good asymptotic results are expected for the higher order modes (TE_{1n} with $n > 1$) even for the moderately small waveguide since in this case $\Omega = \xi'_{1n} > 3$, and for all TM_{1n} modes ($n \geq 1$).

4. CONCLUSIONS

The analysis of the electromagnetic field distribution excited in open-ended circular waveguides has been carried out based on physical optics and incomplete Hankel functions formulation. A line integral representation involving the incomplete Hankel functions has been employed to express the field quantities without introducing analytical or numerical approximations. The exact expressions of the elementary fields involved in the line integral representation allows the analysis of the field distribution near and far from the analyzed structures. In particular, the field distribution computed in closed analytical form along the waveguide axis explicitly show the dependence on the radiative, inductive and electrostatic components as well as the analytical link with the Brillouin's angle related with the Keller's cone. In addition, it has been observed that the uniform asymptotic representation of the $IHFs$ can be employed to determine the field quantities with excellent accuracy on the waveguide axis, except for the TE_{11} and TM_{01} modes. Numerical results concerning the propagation and conversion of the guided-wave modes into the spherical waves have been presented for different exciting modes and waveguide dimensions. It has been observed that interference processes between the guided modes and the field scattered at the waveguide rim are responsible for the electromagnetic energy focusing observed just before the transition of the radiated field toward the spherical wave propagation regime.

ACKNOWLEDGMENT

Mr. M. Fascetti is gratefully acknowledged for his help in the graphical presentation of the results.

APPENDIX A. PARTIAL DERIVATIVES OF THE ELECTRIC VECTOR POTENTIAL

The partial derivatives of the vector potential, needed to compute the electromagnetic field distribution in circular open-ended waveguides excited by non evanescent traveling-wave modes, are given by

$$\frac{\partial}{\partial R}A_0^{\pm}(R,z,z_0) = j\beta_0\gamma_p\frac{1}{4}H_1^{(2)}\left[\beta_0\gamma_p R, sinh^{-1}\left(\frac{\Delta z \mp \alpha_n r_0}{\gamma_p R}\right)\right]e^{\mp j\beta_z z} + \frac{\Delta z}{R}\frac{e^{-j\beta_0 r_0}}{4\pi r_0}e^{\mp j\beta_z z_0}, \quad \text{(A1)}$$

$$\frac{\partial}{\partial z}A_0^{\pm}(R,z,z_0) = \mp\beta_z\frac{1}{4}H_0^{(2)}\left[\beta_0\gamma_p R, sinh^{-1}\left(\frac{\Delta z \mp \alpha_n r_0}{\gamma_p R}\right)\right]e^{\mp j\beta_z z} - \frac{e^{-j\beta_0 r_0}}{4\pi r_0}e^{\mp j\beta_z z_0}, \quad \text{(A2)}$$

$$\frac{\partial^2}{\partial z^2}A_0^{\pm}(R,z,z_0) = j\beta_z^2\frac{1}{4}H_0^{(2)}\left[\beta_0\gamma_p R, sinh^{-1}\left(\frac{\Delta z \mp \alpha_n r_0}{\gamma_p R}\right)\right]e^{\mp j\beta_z z} \pm j\beta_z\frac{e^{-j\beta_0 r_0}}{4\pi r_0}e^{\mp j\beta_z z_0} + \Delta z\left(j\beta_0 + \frac{1}{r_0}\right)\frac{e^{-j\beta_0 r_0}}{4\pi r_0^2}e^{\mp j\beta_z z_0}, \quad \text{(A3)}$$

$$\frac{\partial^2}{\partial R^2}A_0^{\pm}(R,z,z_0) = j\beta_0^2\gamma_p^2\frac{1}{4}H_0^{(2)}\left[\beta_0\gamma_p R, sinh^{-1}\left(\frac{\Delta z \mp \alpha_n r_0}{\gamma_p R}\right)\right]e^{\mp j\beta_z z} - j\beta_0\gamma_p\frac{1}{4R}H_1^{(2)}\left[\beta_0\gamma_p R, sinh^{-1}\left(\frac{\Delta z \mp \alpha_n r_0}{\gamma_p R}\right)\right]e^{\mp j\beta_z z} \mp j\beta_z\frac{e^{-j\beta_0 r_0}}{4\pi r_0}e^{\mp j\beta_z z_0} - \Delta z\left(j\beta_0 + \frac{1}{r_0}\right)\frac{e^{-j\beta_0 r_0}}{4\pi r_0^2}e^{\mp j\beta_z z_0} - \frac{\Delta z}{R^2}\frac{e^{-j\beta_0 r_0}}{4\pi r_0}e^{\mp j\beta_z z_0}, \quad \text{(A4)}$$

$$\frac{\partial^2}{\partial R\partial z}A_0^{\pm}(R,z,z_0) = \pm\beta_z\beta_0\gamma_p\frac{1}{4}H_1^{(2)}\left[\beta_0\gamma_p R, sinh^{-1}\left(\frac{\Delta z \mp \alpha_n r_0}{\gamma_p R}\right)\right] e^{\mp j\beta_z z} \mp j\beta_z\frac{\Delta z}{R}\frac{e^{-j\beta_0 r_0}}{4\pi r_0}e^{\mp j\beta_z z_0} + R\left(j\beta_0 + \frac{1}{r_0}\right)\frac{e^{-j\beta_0 r_0}}{4\pi r_0^2}e^{\mp\beta_z z_0}. \quad \text{(A5)}$$

In (A1)–(A5), the upper/lower sign refers to the progressive/regressive waveguide mode propagation. Notice that the recurrence equation in [13, Eq. (9)] has been employed to derive (A4). This equation shows that in contrast with the derivative of the IHF of order zero, which exhibits the same analytical form of that presented by the conventional Hankel function of order zero [16], the IHF of first order presents additional terms [13, Eq. (9)]. These terms describe spherical waves excited at the current truncation.

APPENDIX B. FIELD COMPONENTS FOR THE TE_{0N} AND TM_{0N} MODES ON THE WAVEGUIDE AXIS

The analytical expressions of field components of the TM_{0n} along the z-axis are

$$E_\rho\left(\rho,\phi,z;z_0\right)\big|_{\rho=0}=0, \tag{B1}$$

$$E_\phi\left(\rho,\phi,z;z_0\right)\big|_{\rho=0}=0, \tag{B2}$$

$$E_z\left(\rho,\phi,z;z_0\right)\big|_{\rho=0}=$$
$$2\pi a\left\{\frac{\omega\mu_0}{4}\gamma_p^2 H_0^{(2)}\left[\beta_0\gamma_p a, sinh^{-1}\left(\frac{\Delta z-\alpha_n r_0}{\gamma_p a}\right)\right]e^{-j\beta_z z}+\right.$$
$$\left.-\left(\eta_0\alpha_n\frac{e^{-j\beta_0 r_0}}{4\pi r_0}+\frac{\Delta z}{j\omega\varepsilon_0}\left(j\beta_0+\frac{1}{r_0}\right)\frac{e^{-j\beta_0 r_0}}{4\pi r_0^2}\right)e^{-j\beta_z z_0}\right\}h_{\phi\,\max}, \tag{B3}$$

while those of the TE_{0n} modes components are

$$H_\rho\left(\rho,\phi,z;z_0\right)\big|_{\rho=0}=0, \tag{B4}$$

$$H_\phi\left(\rho,\phi,z;z_0\right)\big|_{\rho=0}=0, \tag{B5}$$

$$H_z\left(\rho,\phi,z;z_0\right)\big|_{\rho=0}=$$
$$-2\pi a\left\{j\beta_0\gamma_p\frac{1}{4}H_1^{(2)}\left[\beta_0\gamma_p a, sinh^{-1}\left(\frac{\Delta z-\alpha_n r_0}{\gamma_p a}\right)\right]e^{-j\beta_z z}+\right.$$
$$\left.+\frac{\Delta z}{a}\frac{e^{-j\beta_0 r_0}}{4\pi r_0}e^{-j\beta_z z_0}\right\}h_{z\,\max} \tag{B6}$$

with

$$h_{\phi\,\max}=-j\frac{\omega\varepsilon_0}{\zeta_{0n}}aC_0J_0'(\zeta_{0n}), \tag{B7}$$

$$h_{z\,\max}=C_0J_0(\xi_{0n}'). \tag{B8}$$

To derive Eqs. (B1)–(B6) a procedure similar to that adopted in Eqs. (17)–(20) has been employed.

REFERENCES

1. Li, L. W., L. Zhou, M. S. Leong, T. S. Yeo, and P. S. Kooi, "An open-ended circular waveguide with an infinite conducting flange covered by a dielectric hemi-spherical radome shell: Full-wave analysis and Green's dyadics," *Progress In Electromagnetics Research*, PIER 21, 221–245, 1999.
2. Li, B., B. Wu, and C.-H. Liang, "High gain circular waveguide array antenna using electromagnetic band-gap structure," *J. Electromagn. Waves Appl.*, Vol. 20, No. 7, 955–966, 2006.
3. Lo, Y. T. and S. W. Lee, *Antenna Handbook: Theory, Applications and Design*, Van Nostrand Reinhold Company, New York, 1988.
4. Balanis, C. A., *Antenna Theory: Analysis and Design*, John Wiley & Sons, New York, Chichester, Brisbane, Toronto, Singapore, 1982.
5. Jones, D. S., *Acoustic and Electromagnetic Waves*, Clarendon Press, Oxford, 1986.
6. Maci, S., F. Capolino, and F. Mioc, "Line integral representation of the modal radiation for an open-ended waveguide," *IEEE Trans. Antennas Propagat.*, Vol. 45, 1885–1887, Dec. 1997.
7. Ling, H., S. Lee, and R. Chou, "High-frequency RCS of open cavities with rectangular and circular cross sections," *IEEE Trans. Antennas Propagat.*, Vol. 37, 648–654, May 1989.
8. Obelleiro, F., J. L. Rodriguez, and R. J. Burkholder, "An iterative physical optics approach for analyzing the electromagnetic scattering by large open-ended cavities," *IEEE Trans. Antennas Propagat.*, Vol. 43, 356–361, April 1995.
9. Naqvi, Q. A., A. A. Rizvi, and Z. Yaqoob, "Scattering of electromagnetic waves from a deeply burried circular cylinder," *Progress In Electromagnetics Research*, PIER 27, 37–59, 2000.
10. Ruppin, R., "Scattering of electromagnetic radiation by a perfect electromagnetic conductor cylinder," *J. Electromagn. Waves Appl.*, Vol. 20, No. 13, 1853–1860, 2006.
11. Zhong, X.-M., C. Liao, and W. Chen, "Image reconstruction of arbitrary cross section conducting cylinder using UWB pulse," *J. Electromagn. Waves Appl.*, Vol. 21, No. 1, 25–34, 2007.
12. Weinstein, L. A., *The Theory of Diffraction and the Factorization Method*, The Golem Press, Boulder, Colorado, 1969.
13. Cicchetti, R. and A. Faraone, "Incomplete Hankel and modified Bessel functions: a class of special functions for electromagnetics," *IEEE Trans. Antennas and Propagat.*, Vol. 52, No. 12, 3373–3389,

Dec. 2004.

14. Cicchetti, R. and A. Faraone, "On the optical behavior of the electromagnetic field excited by a semi-infinite electric traveling-wave current," *IEEE Trans. Antennas and Propagat.*, Vol. 53, No. 12, 4015–4025, Dec. 2005.
15. Cicchetti, R. and A. Faraone, "Analysis of open-ended circular waveguides using physical optics and incomplete Hankel functions formulation," *IEEE Trans. Antennas and Propagat.*, Vol. 55, No. 6, 1887–1892, June 2007.
16. Watson, G. N., *A Treatise on the Theory of Bessel Functions*, Cambridge University Press, Cambridge, U.K., 1962.